

Optimized multi-level elongated quinary patterns for the assessment of thyroid nodules in ultrasound images

Original

Optimized multi-level elongated quinary patterns for the assessment of thyroid nodules in ultrasound images / Raghavendra, U.; Gudigar, Anjan; Maithri, M.; Gertych, Arkadiusz; Meiburger, Kristen M.; Yeong, Chai Hong; Madla, Chakri; Kongmebhol, Pailin; Molinari, Filippo; Ng, Kwan Hoong; Acharya, U. Rajendra. - In: COMPUTERS IN BIOLOGY AND MEDICINE. - ISSN 0010-4825. - STAMPA. - 95:(2018), pp. 55-62. [10.1016/j.combiomed.2018.02.002]

Availability:

This version is available at: 11583/2701819 since: 2018-02-27T10:37:07Z

Publisher:

Elsevier Ltd

Published

DOI:10.1016/j.combiomed.2018.02.002

Terms of use:

This article is made available under terms and conditions as specified in the corresponding bibliographic description in the repository

Publisher copyright

Elsevier preprint/submitted version

Preprint (submitted version) of an article published in COMPUTERS IN BIOLOGY AND MEDICINE © 2018,
<http://doi.org/10.1016/j.combiomed.2018.02.002>

(Article begins on next page)

Optimized multi-level elongated quinary patterns for the assessment of thyroid nodules in ultrasound images

U Raghavendra^{a*}, Anjan Gudigar^a, Maithri M^b, Arkadiusz Gertych^c, Kristen M. Meiburger^d, Chai Hong Yeong^e, Chakri Madla^f, Pailin Kongmebhol^f, Filippo Molinari^d, Kwan Hoong Ng^e, U Rajendra Acharya^{g,h,i}

^aDepartment of Instrumentation and Control Engineering, Manipal Institute of Technology, Manipal University, Manipal 576104, India.

^bDepartment of Mechatronics Engineering, Manipal Institute of Technology, Manipal University, Manipal 576104, India.

^cDepartment of Surgery, Department of Pathology and Laboratory Medicine, Cedars-Sinai Medical Center, Los Angeles, CA, USA.

^dDepartment of Electronics and Telecommunications, Politecnico di Torino, Italy.

^eDepartment of Biomedical Imaging, University of Malaya, Kuala Lumpur, Malaysia.

^fDepartment of Radiology, Faculty of Medicine, Chiang Mai University, Chiang Mai, 50200, Thailand.

^gDepartment of Electronics and Computer Engineering, Ngee Ann Polytechnic, Clementi 599489, Singapore.

^hDepartment of Biomedical Engineering, School of Science and Technology, SIM University, Clementi 599491, Singapore.

ⁱDepartment of Biomedical Engineering, Faculty of Engineering, University of Malaya, Kuala Lumpur 50603, Malaysia.

*Corresponding Author

Postal Address: Department of Instrumentation and Control Engineering, Manipal Institute of Technology, Manipal University, Manipal 576104, India.

Telephone: (91) 820-2925152; Email Address: U Raghavendra <raghavendra.u@manipal.edu>

Abstract

Ultrasound imaging is one of the most common visualizing tools used by radiologists to identify the location of thyroid nodules. However, visual assessment of nodules is difficult and often affected by inter- and intra-observer variabilities. Thus, a computer-aided diagnosis (CAD) system can be helpful to cross-verify the severity of nodules. This paper proposes a new CAD system to characterize thyroid nodules using

optimized multi-level elongated quinary patterns. In this study, higher order spectral (HOS) entropy features extracted from these patterns appropriately distinguished benign and malignant nodules under particle swarm optimization (PSO) and support vector machine (SVM) frameworks. Our CAD algorithm achieved a maximum accuracy of 97.71% and 97.01% in private and public datasets respectively. The evaluation of this CAD system on both private and public data sets confirmed its effectiveness as a secondary tool in assisting radiological findings.

Keywords: Elongated quinary patterns, higher order spectra, particle swarm optimization, support vector machine, thyroid cancer, ultrasound

1. Introduction

Thyroid cancer is more commonly seen in women compared to men, with the morbidity rate >5% increasing every year [1]. It is estimated that approximately 56,870 new thyroid cancer cases will be diagnosed in 2017 in the United States [2]. Thyroid glands secrete thyroxine (T4) and tri-iodothyronine (T3) hormones that are important for the overall wellbeing of the human body. They mainly regulate metabolism, growth, development, and temperature of the body. They also play a vital role in the development of the brain [3, 4].

Enlargement of the thyroid gland is termed as goiter. Goiters can be either diffuse, i.e., covering the entire gland, or nodular. These thyroid gland “bumps” are referred to as thyroid nodules [5], and can be either benign or malignant. Early diagnosis improves stratification of thyroid nodules and helps in determining the best treatment option [6].

Ultrasound is an inexpensive and effective method in thyroid imaging. Images of the organs are obtained by capturing echoes which are generated as a response to the

sound waves sent from a transducer at a high frequency rate. By analyzing the reflected echoes, it is possible to differentiate healthy and malignant tissues. The ultrasound features of a malignant thyroid nodule include hypoechoic, ill-defined margins and punctate calcification [7]. Ultrasounds also provide a useful tool for disease follow-up in patients with thyroid cancer after treatment.

Thyroid cancer has different stages based on tumor classification without any definitive demarcation between each stage [8]. The “stage” of a cancer refers to a phase in the course of the tumor when it has reached some defined level. Further, computer-aided diagnosis (CAD) of ultrasound images can help the radiologists in early diagnosis of thyroid nodules. The CAD systems often consist of feature extraction and machine learning algorithms. To date, several CADs for thyroid nodule differentiation have been proposed [9-11]. A neural network model described in [12] has gained an accuracy of 88.3%. In [13] an accuracy of 81% is achieved using artificial immune recognition system (AIRS). Directionality patterns implemented in [14] achieved classification accuracy of 89.4%. A neuro-fuzzy classifier proposed in [15] has shown 95.33% accuracy in diagnosing thyroid lesions. Erol et al. [6] concluded in their experiment that radial basis function neural network (RBFNN) is a suitable classifier for thyroid disease compared to multilayer perceptron neural network (MLPNN). An information gain based artificial immune recognition system (IG-AIRS) trained on a dataset with thyroid diseases in [16] yielded an accuracy of 95.90%. A system developed by Dogantekin et al. [17] used principal component analysis (PCA) and support vector machines and obtained 97.67% accuracy. A system described in [18] used discriminant analysis, wavelet features and SVM obtained 91.86% classification accuracy.

The parameters of a SVM classifier were optimized using particle swarm optimization (PSO), and an average accuracy of 97.49% was attained in [19]. PCA was used with an extreme learning machine classifier to obtain new feature space for diseases of the thyroid and achieved a mean accuracy of 97.73%. By adaptively

tweaking the parameters for Fuzzy K-nearest neighbor (FKNN) classifier, the authors of [20] attained a mean accuracy of 98.82%. By applying different scalar validity measures, a comparison of various soft and hard fuzzy clustering techniques was performed for the classification of thyroid disease [21].

A texture feature based technique was developed in [22] and attained a maximum accuracy of 100%. In [23] a new system is developed using combination of discrete wavelet transform (DWT) and texture features with an AdaBoost classifier for the classification of thyroid lesions. 100% accuracy, sensitivity, and specificity are reported by them. Good classification accuracy was shown by grayscale features based on entropy, Gabor wavelet, moments, image texture and higher order spectra (HOS) features [24]. In a work by Acharya et al. [25] to evaluate Hashimoto thyroiditis, a stationary wavelet transform with fuzzy classifier was used and attained a maximum accuracy, sensitivity, specificity of 84.6%, 82.8%, and 87.0% respectively. In [26] Acharya et al. used Gabor transform features with locality sensitive discriminant analysis (LSDA) and C4.5 decision tree classifier to classify benign and malignant thyroid nodules, and attained a maximum accuracy of 94.3%.

Omiotek et al. [27] used linear discriminant analysis classifier to diagnose Hashimoto's thyroiditis and obtained 96.88% sensitivity, 98.44% specificity, and 97.66% overall classification accuracy. Another system was proposed by the same group in [28] which involved a fine-tuned deep convolutional neural network and pre-processed ultrasound images. This system reported the classification performance of 98.29% accuracy, 99.10% of sensitivity and 93.90% specificity using open access database. And obtained 96.34% accuracy, 86% sensitivity, and 99% specificity with non-public database. In [29], an artificial neural network (ANN) was applied to detect thyroid nodules in ultrasound images and obtained 70% accuracy. A more advanced system proposed in [30] utilized a watershed algorithm for the segmentation of nodules and ANN and SVM classifiers for the classification of benign and malignant nodules. The

accuracy, specificity, sensitivity and AUC (area under the curve) were 92.5%, 96.66%, 80%, and 0.91 for SVM and 87.5%, 93.33%, 70% and 0.88 for ANN respectively. The authors of this study concluded that the SVM classifier is more stable and reliable compared to the ANN classifier. In a study involving extraction and classification of elastography features extracted from ultrasound images of thyroid nodules [31], an LDA classifier was used. This was developed to differentiate the thyroid nodules into two types (i) no FNA (fine-needle aspiration) (observation-only) and (ii) FNA. They showed 100% sensitivity and specificity of 75.6% in detecting malignant thyroid nodules. A convolutional neural network (CNN) model was used to extract the deep features from ultrasound images in [32] and achieved 92.9% accuracy in the classification of thyroid nodules. An automated CAD system proposed in [33] consisted of a speckle reduction technique, a procedure to find and segment a region containing suspicious nodules. This segmentation system achieved a true positive of $95.92 \pm 3.70\%$, false positive of $7.04 \pm 4.21\%$, dice coefficient of $93.88 \pm 2.59\%$ and overlap metric of 91.18 ± 7.04 pixels and Hausdorff distance of 0.52 ± 0.20 pixels. Performances of different techniques are collected in Table 5.

However, it is difficult to fairly compare the effectiveness of these techniques because each was tested on different image sets and with different number of subjects in each set. Ideally, the techniques should be tested using large data sets for confirming their effectiveness. Hence, in this work we have developed a new methodology for the characterization of thyroid lesions using optimized HOS entropies extracted from elongated quinary patterns of multi-level gradients. The developed model contains (PSO) and support vector machine (SVM) frameworks and is evaluated on private (288 benign, and 56 malignant) and public (288 benign and 57 malignant) data sets. An overview of the proposed model is shown in Figure 1.

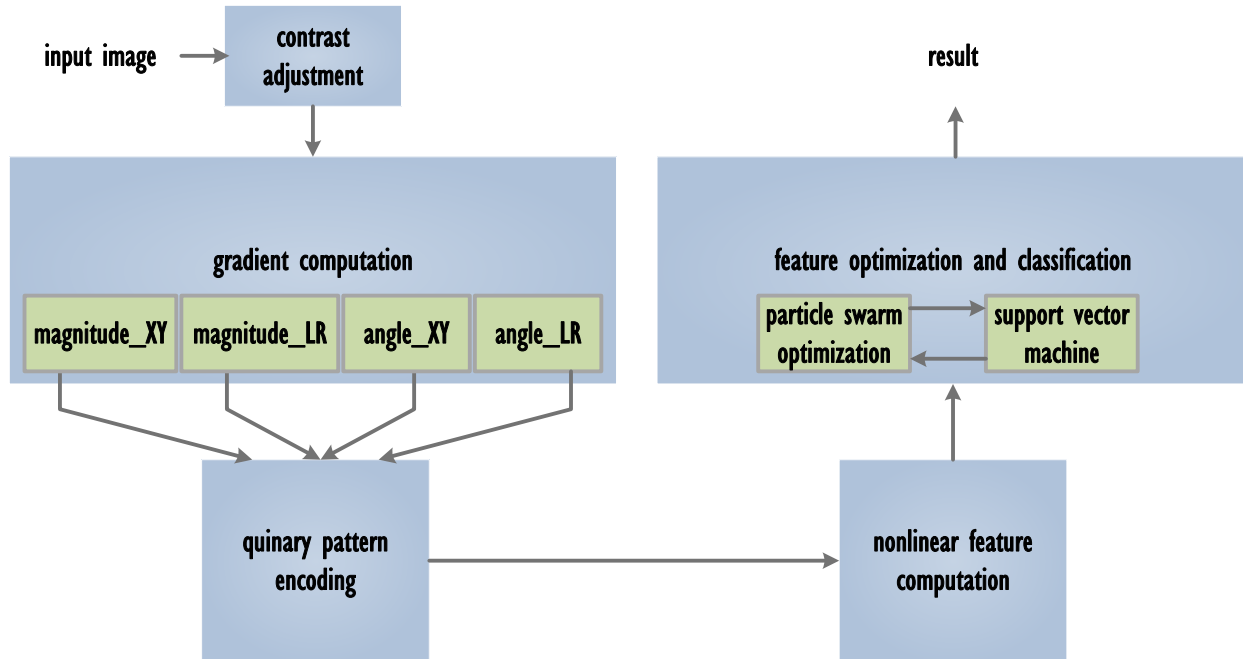


Figure 1. Overview of the proposed model.

2. Material and Methods

2.1 Data Descriptions

In this work, we have used two data sets, one public dataset and another from our own data set.

Data set 1 (Public database): Images are taken from an open-access thyroid ultrasound-image database [34] which consists of ultrasound images of thyroid nodules. From this publically available database, 288 benign and 57 malignant images belong to 99 controls and 200 cases were considered with age range of $57:35 \pm 16:2$ years. The ultrasound image sequences were captured with TOSHIBA Nemio 30 and TOSHIBA Nemio MX ultrasound systems, both set to 12 MHz convex and then from this sequence, thyroid images were extracted. The patients were individually evaluated by two experts and the TI-RAD lexicon description was provided [35].

Data set 2 (Private database): This is a private data set collected at Chiang Mai University Hospital between December 1st, 2009 and December 31st, 2016. Cytology (by fine needle aspiration biopsy) or surgical excision were used to confirm the presence of benign or malignant nodules. In this study, 344 thyroid nodule images were collected, out of which 288 were benign, and 56 were malignant. The images were collected from patients between 12 and 88 years of age (mean age: 44.1 years). The patients were examined using one of the following scanners: GE LOGIQ 9 and LOGIQ E9 with linear transducer 10–14 MHz, SIEMENS Acuson Sequoia 512 with linear transducer 5–13 MHz, TOSHIBA Aplio-XG with linear transducer 10–13 MHz and PHILIPS iU22 with linear transducer 5–15 MHz, depending on scanner availability. B-Mode images were collected during the examination.

2.2 Feature representation using quinary encoding

Multi-level gradients are effective and robust feature representation techniques in image analysis [36]. Multi-gradient magnitudes and angles are derived from a given image in XY and left-right (LR) directions. To extract gradient components, four different Sobel masks were used in various orientations, and the resultant images were used to compute the magnitude and angle of the gradient.

To obtain the gradient in the XY direction, Pixels around the center pixel P_{x5} of a sub image of size 3x3 are convolved with the horizontal (H_m) and vertical (V_m) Sobel masks.

$$Gr_x(H) = (P_{x1} + 2P_{x2} + P_{x3}) - (P_{x7} + 2P_{x8} + P_{x9}) \quad (1)$$

Where, the $Gr_x(H)$ represents the horizontal direction gradient of pixel P_{x5} .

Similarly, the gradient of pixel P_{x5} in vertical direction is given by:

$$Gr_y(V) = (P_{x1} + 2P_{x4} + P_{x7}) - (P_{x3} + 2P_{x6} + P_{x9}) \quad (2)$$

Using the $Gr_x(H)$ and $Gr_y(V)$ components, the magnitude gradient $Gmag_{xy}$ and angle gradient $Gdir_{xy}$ are computed. Magnitude gradient is given by

$$Gmag_{xy} = |Gr_x(H)| + |Gr_y(V)| \quad (3)$$

And angle gradient is

$$Gdir_{xy} = \tan^{-1} \left(\frac{Gr_y(V)}{Gr_x(H)} \right) \quad (4)$$

Likewise, to obtain the magnitude and angle gradients for the center pixel P_{x5} in L-R direction the center pixel is convolved with the diagonal masks D_1 and D_2 . The gradient of the pixel P_{x5} left (l) and right (r) is given by

$$Gr_l(d2) = (P_{x2} + 2P_{x3} + P_{x6}) - (P_{x4} + 2P_{x7} + P_{x8}) \quad (5)$$

And

$$Gr_r(d1) = (P_{x6} + 2P_{x9} + P_{x8}) - (2P_{x1} + P_{x2} + P_{x4}) \quad (6)$$

Using these convolution outputs, magnitude gradient $Gmag_{LR}$ and angle gradient $Gdir_{LR}$ are obtained as follows:

$$Gmag_{LR} = |Gr_l(d2)| + |Gr_r(d1)| \quad (7)$$

$$Gdir_{LR} = \tan^{-1} \left(\frac{Gr_r(d1)}{Gr_l(d2)} \right) \quad (8)$$

Figure 2 shows the extracted gradient magnitude and angle in both the XY and LR directions.

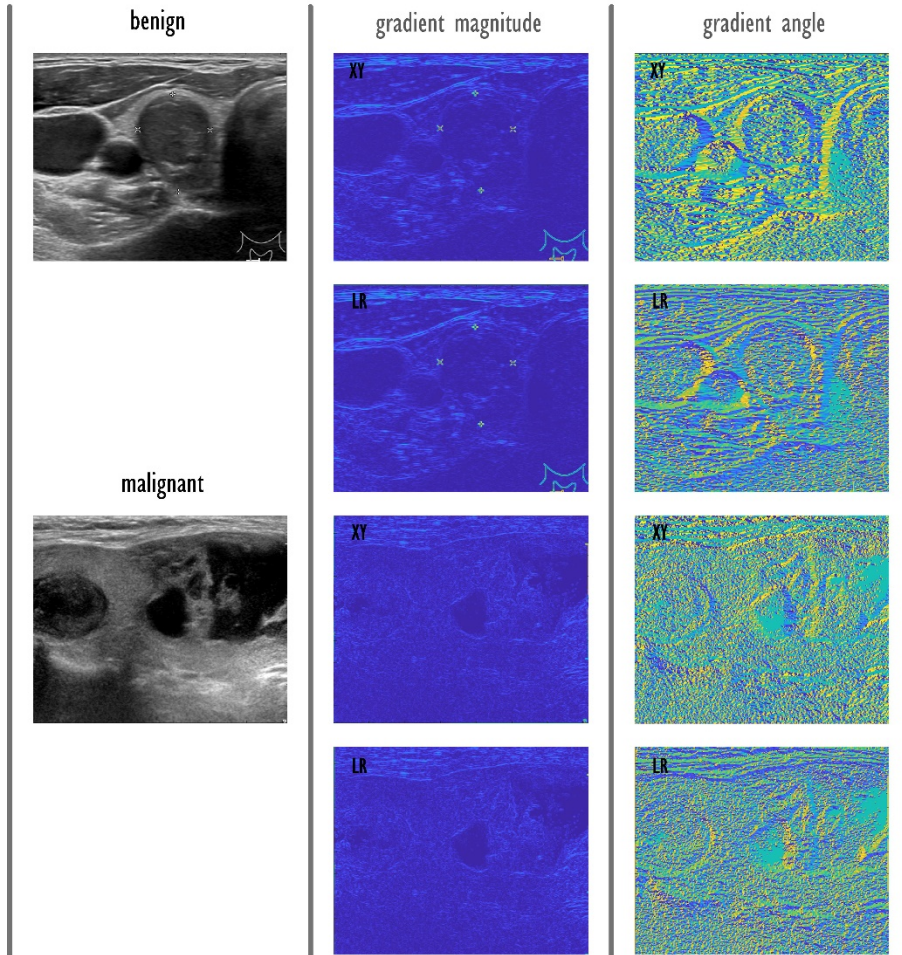


Figure 2. Magnitude and angle in two different directions.

Regions which have rough versus smooth textures can be isolated using gradient feature extraction technique. The magnitude gradient features are stable and consistent in the edge and curve regions in images with rough textures. Hence, it becomes easier to isolate regions with the higher intensity regions. The angle gradient features explore the minute features such as bump or swelling at different angles.

The LR and XY gradient magnitudes and angles (eight gradient components) are quantized with an elongated quinary pattern (EQP) technique and five levels of encoding [36]. To encode the eight-connected pixel neighborhood, two threshold values Th_1 and Th_2 , are involved. Various combinations of values were used for Th_1 and Th_2

ranging from 1 to 20 and the performance was observed. The values 4 and 9 for Th_1 and Th_2 respectively showed better performance.

The five-level encoding in terms of gradient magnitude as:

$$Gr_{mag_{EQP}}(Gr_{mag_p}, Gr_{mag_c}) : \begin{cases} +2 & Gr_{mag_p} \geq Gr_{mag_c} + Th_2 \\ +1 & Gr_{mag_c} + Th_1 \leq Gr_{mag_p} < Gr_{mag_c} + Th_2 \\ 0 & Gr_{mag_c} - Th_1 \leq Gr_{mag_p} < Gr_{mag_c} + Th_1 \\ -1 & Gr_{mag_c} - Th_2 \leq Gr_{mag_p} < Gr_{mag_c} - Th_1 \\ -2 & otherwise \end{cases}$$

Where Gr_{mag_p} signifies the gradient magnitudes of neighboring points which are surrounding this center pixel gradient magnitude (Gr_{mag_c}).

Figure 3 shows an example of encoded quinary patterns of magnitude and angle in both the XY and LR direction. **Figure 4** shows the EQP of benign and malignant classes.

image patch			Gmag_XY			Gmag_LR			Gdir_XY			Gdir_LR		
103	122	110	876	678	590	886	771	543	99	124	116	148	160	73
97	107	103	567	601	122	667	529	237	107	119	109	156	154	77
110	109	113	606	595	94	530	580	80	86	89	126	130	137	145
EQP encoding														
2	2	-2	2	2	2	-2	1	0	-1	1	-2			
-2		-2	2		-2	-2		-2	0		-2			
1	-1	-2	0	2	-2	-2	-2	1	-2	-2	-1			

Figure 3. Example of elongated quinary pattern descriptor.

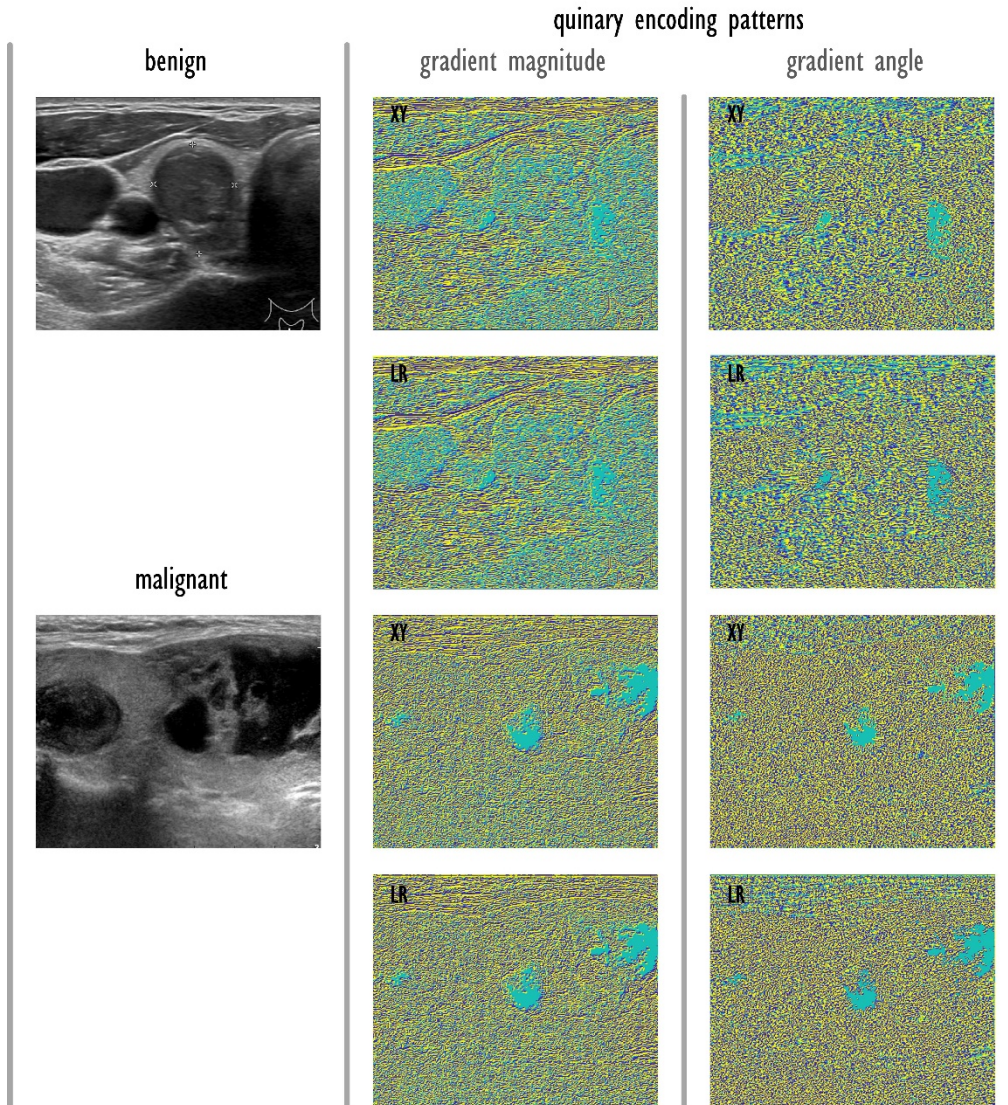


Figure 4. Elongated quinary patterns of magnitude and angle gradients for example benign and malignant nodules.

2.3 Higher order spectral entropies

Higher order spectra (HOS) are designed for the better spectral representation of stochastic or deterministic processes. HOS analysis is very useful in the identification of non-linearity in deterministic signals and random processes [37-39]. It has been shown that HOS analysis has many potential applications in medical image analysis [40], traffic sign recognition [41], etc. Generally, a bispectrum of 2-D signals can be characterized in 4-D. For example, a HOS analysis is a 1-D projection of an image performed for a given

angle θ using the Radon transform (RT). Based on the RT and bispectra, features such as bispectral first, second and third entropy are extracted as defined in [40]. The phase entropy can also be extracted from bispectrum.

Finally, adaptive synthetic (ADASYN) sampling is used to alleviate the problem of imbalance in sample number between two classes. ADASYN uses the density distribution to determine the number of samples required for the class of minimum samples. The resultant balanced samples with features can be used for further processing [42].

2.4 Feature Selection and Classification

PSO is a population-based search method proposed by Kennedy and Eberhart to mimic the flocking behavior of birds and fish swarms [43]. In PSO, the positions of every particle of a given swarm (i.e., population) is updated based on the previous experiences. After the update, new fitness values of these particles are calculated. This process continues until stopping criteria are met. PSO was used to select 5, 10, 15, 20, and 25 top features that were fed to an SVM classifier [44, 45], as it has the capacity to generalize by optimizing the margin [46]. The classifier performance was tested with 1st, 2nd and 3rd polynomial, and radial basis function (RBF) kernels to find the best performing classifier. We have considered accuracy, sensitivity and specificity as our performance evaluation metrics.

3. Experimental Results

In this study, we have used both public (Benign: 288, Malignant: 57) and private (Benign: 288, Malignant: 56) ultrasound thyroid data sets to develop, and assess the performance of thyroid nodule differentiation. The processing begins with the calculation of multi-level gradient magnitudes and angles in the XY-direction and LR-direction, and yielded *four* different gradient components. Each gradient component is

encoded using quinary encoding patterns and their corresponding *seventy two* higher order spectral entropies are extracted ($72 \times 4 = 288$ features). In order to overcome the imbalance in number of observations between benign and malignant classes, the ADASYN is used. It has created *two hundred twenty four* additional synthetic minority data samples for public as well as private data sets. These features are subjected to PSO to select the most significant features for classification. We have used SVM classifier with different kernel functions for classification. Ten-fold cross validation is used to evaluate the performance of the developed system.

We have performed our experiments by selecting 5, 10, 15, 20 and 25 selected significant features with various iterations which randomly selects different features using PSO and SVM. The features with maximum accuracy are further used for 10-fold cross validation. The obtained classification performances for different kernel functions are given in Tables 1 and 2. We have achieved an average performance of 93.89% accuracy, 88.85% sensitivity and 94.66% specificity for the combination of *fifteen* iterations and *ten* features using a public data set. We have also achieved average performance of 91.91% accuracy, 92.85% sensitivity and 88.54% for the combination of *twenty* iterations and *ten* features with a private data set. In order to test the usefulness of quinary patterns, we have extracted HOS entropies directly from multi-level gradients and fed them to PSO-SVM combination for classification. The obtained results are presented in Tables 3 and 4 for public and private data sets respectively. The average accuracy of 89.92% is achieved for *ten* significant features with *twenty* iterations using the public data set. It can be observed that the model performed better when HOS entropies are extracted from quinary patterns rather than from gradients. Figures 5 and 6 shows the maximum performance of the proposed model for different combinations of features and iterations for both public and private data sets.

Table 1: Performance of proposed model for different kernels for public data set.

SVM Kernel	Iterations	Features	Accuracy (%)	Sensitivity (%)	Specificity (%)
Poly 1	15	10	65.55	61.67	69.75
Poly 2	15	10	76.62	64.45	89.32
Poly 3	15	10	77.50	60.27	95.37
RBF	15	10	93.89	88.85	94.66

Table 2: Performance of proposed model for different kernels for private data set.

SVM Kernel	Iterations	Features	Accuracy (%)	Sensitivity (%)	Specificity (%)
Poly 1	20	10	59.15	60.71	57.63
Poly 2	20	10	70.59	81.42	60.06
Poly 3	20	10	80.28	93.92	67.01
RBF	20	10	91.91	92.85	88.54

Table 3: Performance of HOS entropy extracted from multi-level gradient for different kernels using the public data set.

SVM Kernel	Iterations	Features	Accuracy (%)	Sensitivity (%)	Specificity (%)
Poly 1	20	10	56.82	57.14	60.14
Poly 2	20	10	69.96	64.80	79.71
Poly 3	20	10	72.18	56.09	93.23
RBF	20	10	89.92	82.57	90.39

Table 4: Performance of HOS entropy extracted from multi-level gradient for different kernels using private data set.

SVM Kernel	Iterations	Features	Accuracy (%)	Sensitivity (%)	Specificity (%)
Poly 1	15	10	60.51	60.60	60.41
Poly 2	15	10	71.79	79.46	63.88
Poly 3	15	10	80.17	95.95	63.88
RBF	15	10	91.78	92.25	85.06

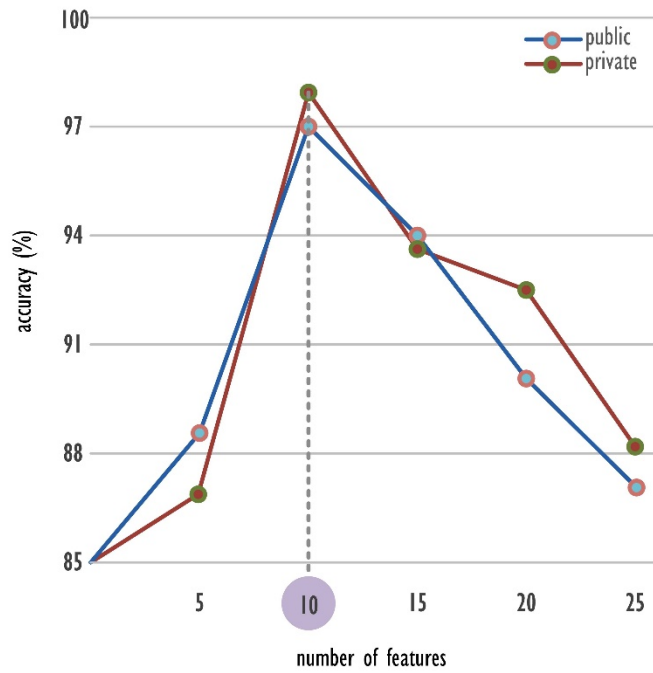


Figure 5. Performance of the proposed model for change in features with fixed iteration of 10.

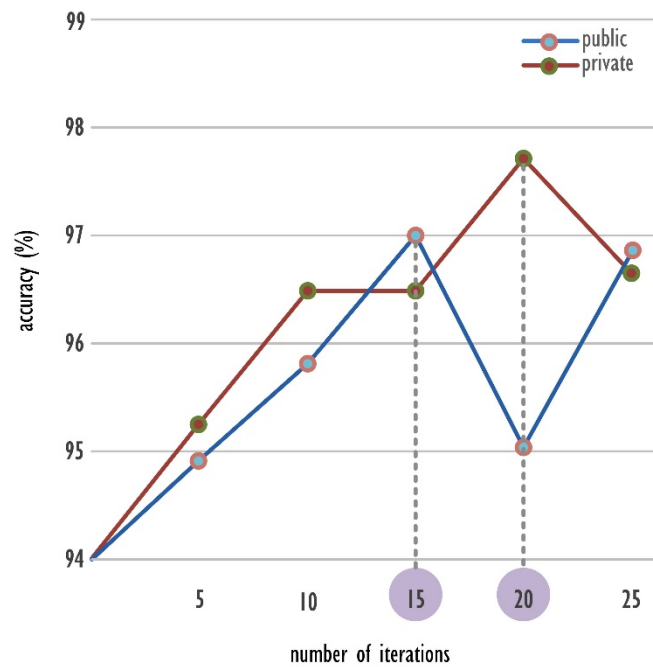


Figure 6. Performance of the proposed model for change in iteration with fixed features of 10.

4. Discussion

Ultrasound is the most commonly used modality for the detection and assessment of thyroid nodules. In this study, we have presented a novel methodology for the characterization of thyroid nodules that belong to either the benign or malignant group. We have used encoded quinary patterns of magnitude and angle gradients in two different directions to extract the features and classify the nodules. The gradient magnitudes are effective to characterize a textured or regions with curvatures whereas angle magnitudes explore minute features such as bumps or swelling at different orientations [36]. The enhanced gradients are systematically encoded using elongated quinary patterns which automatically reduce the gradient sensitivity by quantizing and encoding in the key regions of thyroid images. The obtained entropy features from these patterns can discriminate benign and malignant lesions during classification. In addition, the ADASYN synthetic sample generation algorithm has compensated the issue of imbalanced samples which helps to prevent the over-fitting of classifier. The extracted features with synthetic samples are fed to the PSO algorithm to select these best features. These selected features were used to train the SVM classifier. Our system required only *ten* significant features from the extracted 288 features to attain 93.89% average accuracy. In order to test the robustness of our model, we have also repeated our experiment using public database and different kernel functions. It is observed that the SVM with RBF kernel has attained maximum performance in all combinations as shown in Tables 1 and 2. We have also observed the superiority of extracting HOS features from EQP patterns than extracting it from multi-level gradients as shown in Tables 3 and 4 as it compensates the gradient sensitivity [36]. Overall performance is boosted approximately by 4% for the public dataset. Figures 5 and 6 show the maximum result obtained using PSO and SVM. It is observed that the proposed system attained a maximum accuracy of 97.71% and 97.01% for private and public datasets respectively. The major observation during our experiment is that the performance of

the developed model is consistent for both public and private data sets irrespective of using the imbalanced data in both private and public datasets (benign patients are more than malignant). Our study used images from public and private repositories and compared with other studies published to date on this topic (Table 5).

Table 5: State-of-the-art techniques on characterization of thyroid lesions.

Papers	No. of Subjects	Method / Classifier	Accuracy (%)
[12]	215	MLP+RBF+CSFNN	88.3, 81.69 and 85.92
[47]	66	Radon Transform + SVM	89.4
[13]	215	AIRS	81
[14]	66	Radon Transform + SVM	89.4
[15]	215	Neuro Fuzzy classifier	95.33
[16]	215	IG-AIRS	95.90
[48]	85	Morphological+ Wavelet features + SVM	AUC: 0.96
[17]	215	PCA+SVM	97.67
[49]	98	k-means clustering + PCA + SVM	87.8
[50]	61	Texture features + SVM	100
[51]	200	Fuzzy local binary patterns + fuzzy grey-level histogram features + SVM	97.5
[18]	215	Discriminant Analysis + Wavelet + Support Vector Machine	91.86
[19]	215	PSO+SVM	97.49
[20]	215	Fuzzy k-nearest neighbor	98.82
[52]	125	Hard area ratio + textural features + SVM	93.6
[53]	142	Textural + shape feature vectors + SVM	AUC: 0.93
[54]	13	GLCM+SVM	84.62
[55]	118	Noise resilient features + SVM	95.2
[22]	10	Texture Feature + SVM	100
[23]	10	DWT + texture + AdaBoost	100
[26]	242	Gabor transform + LSDA + C4.5 decision tree classifier	94.3
[56]	242	Fractal + SGLDF + MFA	97.52

5. Conclusion

In this paper, a novel automated CAD system is proposed to characterize thyroid nodules. Our CAD achieved 97.71% maximum accuracy using only *ten* features. The HOS entropies extracted from multi-level elongated quinary patterns delineates the non-linearity among benign and malignant classes thereby providing the best discrimination of nodules. The PSO-SVM framework helped to select the most significant features, and achieve maximum performance with minimum features. The developed system is robust as it gives highest performance for both private and public data sets with the same number of features. This CAD can be used as a screening tool to assist the clinicians during their routine checkups of thyroid nodules.

References

1. Miller KD, Siegel RL, Lin CC, et al. Cancer treatment and survivorship statistics, 2016. *CA Cancer J Clin.* 66 (2016) 271-289.
2. American Cancer Society, <https://www.cancer.org/cancer/thyroid-cancer/about/key-statistics.html> (Last Accessed: 13.05.2016).
3. H.J. Biersack, F. Grünwald, *Thyroid Cancer*, second ed., Springer, Berlin, 2005.
4. <https://www.quora.com/Why-is-Thyroxine-called-the-personality-hormone>] (Last accessed: 30.10.2017)
5. <https://www.cancer.org/cancer/thyroid-cancer/about/what-is-thyroid-cancer.html>] (Last accessed: 30.10.2017)
6. R. Erol, S.N. Ogulata, C. Sahin, Z.N. Alparslan, A radial basis function neural network (rbfn) approach for structural classification of thyroid diseases, *J. Med. Syst.* 32 (3) (2008) 215–220.
7. K T Wong and Anil T Ahuja, Ultrasound of thyroid cancer, *Cancer imaging*, 5(1), 2005, 157–166.
8. Wartofsky L. (2016) Staging of Thyroid Cancer. In: Wartofsky L., Van Nostrand D. (eds) *Thyroid Cancer*. Springer, New York, NY

9. U. R. Acharya, G Swapna, S Vinitha Sree, F Molinari, S Gupta, RH Bardales, A Witkowska, JS Suri, A Review on Ultrasound-based Thyroid Cancer Tissue Characterization and Automated Classification, *Technology in Cancer Research and Treatment*, 13(4), 2014, 289–301.
10. L.N. Li, J.H. Ouyang, H.L. Chen, D.Y. Liu, A computer aided diagnosis system for thyroid disease using extreme learning machine, *J. Med. Syst.* 36 (5) (2012) 3327–3337.
11. V.K. Sudarshan, M.R.K. Mookiah, U.R. Acharya, V. Chandran, F. Molinari, H. Fujita, K.H. Ng, Application of wavelet techniques for cancer diagnosis using ultrasound images: a review, *Comput. Biol. Med.* 69 (2016) 97–111.
12. L. Ozyilmaz, T. Yildirim, Diagnosis of thyroid disease using artificial neural network methods, in: *Proceedings of the 9th International Conference on in Neural Information Processing*, 2002, pp. 2033–2036.
13. K. Polat, S. Sahan, S. Gunes, A novel hybrid method based on artificial immune recognition system (airs) with fuzzy weighted pre-processing for thyroid disease diagnosis, *Expert Syst. Appl.* 32 (4) (2007) 1141–1147.
14. M.A Savelonas, D.K Iakovidis, N. Dimitropoulos, D. Maroulis, Computational characterization of thyroid tissue in the radon domain, in: *20th IEEE International Symposium on Computer Based Medical Systems*, 2007, pp. 189–192.
15. A. Keles, A. Keles, ESTDD: Expert system for thyroid diseases diagnosis, *Expert Syst. Appl.* 34 (1) (2008) 242–246.
16. H. Kodaz, S. Ozsen, A. Arslan, S. Gunes, Medical application of information gain based artificial immune recognition system (airs): diagnosis of thyroid disease, *Expert Syst. Appl.* 36 (2) (2009) 3086–3092.
17. E. Dogantekin, A. Dogantekin, D. Avci, An automatic diagnosis system based on thyroid gland: ADSTG, *Expert Syst. Appl.* 37 (9) (2010) 6368–6372.
18. E. Dogantekin, A. Dogantekin, D. Avci, An expert system based on generalized discriminant analysis and wavelet support vector machine for diagnosis of thyroid diseases, *Expert Syst. Appl.* 38 (1) (2011) 146–150.
19. H.L. Chen, B. Yang, G. Wang, J. Liu, Y.D. Chen, D.Y. Liu, A three-stage expert system based on support vector machines for thyroid disease diagnosis, *J. Med. Syst.* 36 (3) (2011) 1953–1963.
20. D.Y. Liu, H.L. Chen, B. Yang, X.E. Lv, L.N. Li, J. Liu, Design of an enhanced fuzzy knearest neighbor classifier based computer aided diagnostic system for thyroid disease, *J. Med. Syst.* 36 (5) (2011) 3243–3254.

21. A.T. Azar, S.A. El-Said, A.E. Hassanien, Fuzzy and hard clustering analysis for thyroid disease, *Comput. Methods Programs Biomed.* 111 (1) (2013) 1–16.
22. U.R. Acharya, S.V. Sree, M.M.R. Krishnan, F. Molinari, R. Garberoglio, J.S. Suri, Non-invasive automated 3D thyroid lesion classification in ultrasound: a class of thyroscan systems, *Ultrasonics* 52 (4) (2012) 508–520.
23. U.R. Acharya, O. Faust, S.V. Sree, F. Molinari, J.S. Suri, Thyroscreen system: high resolution ultrasound thyroid image characterization into benign and malignant classes using novel combination of texture and discrete wavelet transform, *Comput. Methods Programs Biomed.* 107 (2) (2012) 233–241.
24. U.R. Acharya, S.V. Sree, M.R.K. Mookiah, R. Yantr, F. Molinari, W. Zielez'nik, J. Malyszek-Tumidajewicz, B. Stepien, R.H. Bardales, A. Witkowska, J.S. Suri, Diagnosis of hashimotos thyroiditis in ultrasound using tissue characterization and pixel classification, *J. Eng. Med.* 227 (7) (2013) 788–798.
25. U.R. Acharya, S.V. Sree, M.R.K. Mookiah, F. Molinari, W. Zielenik, R.H. Bardales, A. Witkowska, J.S. Suri, Computer aided diagnostic system for detection of hashimoto thyroiditis on ultrasound images from a polish population, *J. Ultrasound Med.* 33 (2) (2014) 245–253.
26. U.R. Acharya, P. Chowriappa, H. Fujita, S. Bhat, S. Dua, J.E.W. Koh, L.W.J. Eugene, P. Kongmebhol, K.H. Ng, Thyroid lesion classification in 242 patient population using gabor transform features from high resolution ultrasound images, *Knowl. Based Syst.* 171 (2016) 235–245.
27. Zbigniew Omiotek Fractal analysis of the grey and binary images in diagnosis of Hashimoto's thyroiditis, *Biocybernetics and Biomedical Engineering*, 37(4), 2017, 655-665
28. Jianning Chi1 & EktaWalia & Paul Babyn & Jimmy Wang & Gary Groot & Mark Eramian, Thyroid Nodule Classification in Ultrasound Images by Fine-Tuning Deep Convolutional Neural Network, *J Digit Imaging* (2017) 30:477–486
29. Priti S. Dhaygude, S. M. Handore, Detection of Thyroid Nodule in Ultrasound Images Using Artificial Neural Network, *International Journal of Advanced Computational Engineering and Networking*, 4(2), 2016
30. Gireesha H M, Nanda S, Thyroid Nodule Segmentation and Classification in Ultrasound Images, *International Journal of Engineering Research & Technology (IJERT)*, 3(5), 2014
31. SiLuo, Eung-HunKim, ManjiriDighe, YongminKim, Thyroid nodule classification using ultrasound elastography via linear discriminant analysis. *Ultrasonics*, Volume 51, Issue 4, May 2011, Pages 425-431

32. Tianjiao Liu, Shuaining Xie, Yukang Zhang, Jing Yu, Lijuan Niu, Weidong Sun, Feature Selection And Thyroid Nodule Classification Using Transfer Learning, IEEE 14th International Symposium on Biomedical Imaging (ISBI 2017).
33. DeepikaKoundal, Savita Gupta, Sukhwinder Singh, Computer-aided thyroid nodule detection system using medical ultrasound images, , Biomedical Signal Processing and Control, 40, 2018, Pages 117-130
34. Lina Pedraza, Carlos Vargas, Fabian Narvaez, Oscar Duran, Emma Muñoz and Eduardo Romero. An open access thyroid ultrasound-image Database 10th International Symposium on Medical Information Processing and Analysis, SPIE 9287, 2015.
35. Jianning Chi & EktaWalia & Paul Babyn & Jimmy Wang & Gary Groot & Mark Eramian, Thyroid Nodule Classification in Ultrasound Images by Fine-Tuning Deep Convolutional Neural Network, J Digit Imaging (2017) 30:477–486.
36. S.A.M. Al-Sumaidae, M.A.M. Abdullah, R.R.O. Al-Nima, S.S. Dlay, J.A. Chambers, Multi-gradient features and elongated quinary pattern encoding for image-based facial expression recognition, Pattern Recognition 71 (2017) 249–263.
37. Y.C. Kim, E.J. Powers, Digital bispectral analysis and its applications to nonlinear wave interactions, IEEE Trans. Plasma Sci. 7 (1979) 120-131.
38. G.B. Giannakis, Cumulants: a powerful tool in signal processing, Proc. IEEE 75 (1987) 1333-1334.
39. V. Chandran, S. Elgar, Bispectral analysis of two-dimensional random processes, IEEE Trans. Acoust. Speech Signal Process. 38 (1990) 2181-2186.
40. K.C. Chua , V. Chandran , U.R. Acharya , C.M. Lim , Cardiac state diagnosis using higher order spectra of heart rate variability, J. Med. Eng. Technol. 32 (2) (2008) 145–155
41. Anjan Gudigar, Shreesha Chokkadi , U. Raghavendra , U. Rajendra Acharya,“ Local texture patterns for traffic sign recognition using higher order spectra”, Pattern Recognition Letters 94 (2017) 202–210.
42. Haibo He, Yang Bai, Edwardo A. Garcia, and Shutao Li “ADASYN: Adaptive Synthetic Sampling Approach for Imbalanced Learning” 2008 IEEE International Joint Conference on Neural Networks 2008, 1322-1328, Hong Kong, China.
43. J. Kennedy, R. Eberhart, Particle swarm optimization, in: Proceedings of the Sixth International Symposium on Micro Machine and Human Science, Nagoya, Japan, 1995, pp. 39–43.
44. R. Batuwita, V. Palade, Class Imbalance Learning Methods for Support Vector Machines, In Imbalanced Learning: Foundations, Algorithms and Applications, Haibo He and Yunqian Ma Ma (Eds.), Wiley, 2013.

45. R. Akbani, S. Kwek, N. Japkowicz, Applying Support Vector Machines to Imbalanced Datasets, in: Proceedings ECML, 2004, 39–50.
46. C.J.C. Burges, A Tutorial on Support Vector Machines for Pattern Recognition Data Min. Knowl. Discov., Kluwer Academic Publishers 2, 1998, pp. 121–167.
47. M.A. Savelonas, D.K. Iakovidis, N. Dimitropoulos, D. Maroulis, Computational characterization of thyroid tissue in the radon domain, in: Proceedings of 12th IEEE International Symposium on Computer-Based Medical Systems, Slovenia, 2007, pp. 189–192.
48. S. Tsantis, N. Dimitropoulos, D. Cavouras, G. Nikiforidis, Morphological and wavelet features towards sonographic thyroid nodules evaluation, Comput. Med. Imag. Graph. 33 (2009) 91–99.
49. J. Ma, S. Luo, M. Dighe, D. Lim, Y. Kim, Differential diagnosis of thyroid nodule with ultrasound elastography based on support vector machines, in: International Ultrasonics Symposium, 2010, pp. 1372–1375.
50. C.Y. Chang, S.J. Chen, M.F. Tsai, Application of support-vector-machine-based method for feature selection and classification of thyroid nodules in ultrasound images, Pattern Recogn. 43 (2010) 3494–3506.
51. D.K. Iakovidis, E.G. Keramidas, D. Maroulis, Fusion of fuzzy statistical distributions for classification of thyroid ultrasound patterns, Artif. Intell. Med. 50 (1) (2010) 33–41.
52. J. Ding, H. Cheng, C. Ning, J. Huang, Y. Zhang, Quantitative measurement for thyroid cancer characterization based on elastography, J. Ultrasound Med. 30 (9) (2011) 1259–1266.
53. I.N. Legakis, M. Savelonas, D.E. Maroulis, D. Iakovidis, Computer-based nodule malignancy risk assessment in thyroid ultrasound images, Int J. Comput. Appl. 33 (1) (2011) 29–35.
54. N. Singh, A. Jindal, Ultra sonogram images for thyroid segmentation and texture classification in diagnosis of malignant (cancerous) or benign (noncancerous) nodules, Int. J. Eng. Innovative Technol. 1 (5) (2012) 202–206.
55. E.G. Keramidas, D. Maroulis, D.K. Iakovidis, TND: a thyroid nodule detection system for analysis of ultrasound images and videos, J. Med. Syst. 36 (2012) 1271–1281.
56. U. Raghavendra, U. Rajendra Acharya, Anjan Gudigar, Jen Hong Tan, Hamido Fujita, Yuki Hagiwara, Filippo Molinari, Pailin Kongmebhol, Kwan. Hoong Ng, Fusion of Spatial Gray Level Dependency and Fractal Texture Features for the Characterization of Thyroid Lesions, Ultrasonics, 77 (2017) 110–120.